Heat Capacity for the Binary System of Quercetin and Poly(vinylpyrrolidone) K30

Yu-Li Li,[†] Yan Yang,[†] Tong-Chun Bai,*[,†] and Jian-Jun Zhu[‡]

College of Chemistry, Chemical Engineering and Materials Science, Soochow University, Suzhou 215123, China, and Department of Chemistry, State University of New York, Stony Brook, New York 11796, United States

Solid dispersions and mixtures of quercetin and poly(vinylpyrrolidone) (PVP) K30 are studied by differential scanning calorimetry (DSC), X-ray powder diffraction (XRD), Fourier transform infrared spectroscopy (FT-IR), and heat capacity (C_p) measurements. The IUPAC name for PVP is 1-ethenylpyrrolidin-2-one, and that for quercetin is 2-(3,4-dihydroxyphenyl)-3,5,7-trihydroxy-4*H*-1-benzopyran-4-one. A solid dispersion is found in the region of $w_1 < 0.5$, and a solid mixture is found in the region of $w_1 > 0.5$, where w_1 is the mass fraction of quercetin. The C_p data is correlated to temperature T by a polynomial equation, and changes in enthalpy and entropy were calculated from C_p. The C_p data is valuable in the evaluation of drug efficiency.

Introduction

Flavonoids, especially flavonols, have recently been studied extensively for their antioxidant[1−3] and chelating properties.[4] Owing to their phenolic nature, flavonoids are quite polar but poorly water-soluble. Quercetin, with its molecular structure given in Figure 1 and an IUPAC name of 2-(3,4-dihydroxyphenyl)-3,5,7-trihydroxy-4*H*-1-benzopyran-4-one, is one of the most common flavonols present in nature. It has gained the attention of many researchers because of its biological and medicinal applications.[5−12] However, its poor solubility in water limits its dissolution and bioavailability when administered orally. To improve the solubility and dissolution rate of hydrophobic drugs, a variety of methods have been developed, including a biochemical synthesis method,[6,7] an inclusion complex method,[8−11] and a solid dispersion method.[12]

Solid dispersion is one of the most promising methods of improving the solubility and dissolution rate of hydrophobic drugs. It improves the drug wetability and bioavailability[13] by reducing the drug particle size to a minimum scale. The solubilization efficiency of a solid dispersion depends on a multitude of properties of compound and experimental factors. The crystalline state and the particle size of the drug depend on the mixing conditions in the process of preparing solid dispersions. During drug dissolution in water, the dissolution rate is determined partially by the solid state because the crystal lattice of the compound has been disrupted first. Generally speaking, an amorphous drug always exhibits a higher solubility in solvents than does a crystalline drug.[14,15] Therefore, it is important to study a solid dispersion in pharmaceutical applications.

Poly(vinylpyrrolidone) (PVP), with the IUPAC name 1-ethenylpyrrolidin-2-one, is one of the most common compounds in making a solid dispersion drug.[12,16] Its amorphous solid state promotes the drug solubility and dissolution rate. During preparation and medicinal application, the most important thing is to study the phase state of solid mixtures. To address this problem, the dependence of the phase state on the composition and temperature must be known. Among many physical properties, the heat capacity is essential to studying the phase transition, critical phenomena, and glass transition.[17−20] Therefore, basic data originates from an evaluation of the efficiency of drugs.

In this article, solid dispersions and mixtures of (quercetin + PVP K30) were prepared by a solvent evaporation method.[21] The phase state of these mixtures was studied by differential scanning calorimetry (DSC), X-ray powder diffraction (XRD), and Fourier transform infrared spectroscopy (FT-IR). By measuring the heat capacity of this binary system, information on the phase state and the conditions used to prepare a solid dispersion drug can be obtained.

Experimental Section

Materials. Quercetin (CAS no. 117-39-5, with IUPAC name 2-(3,4-dihydroxyphenyl)-3,5,7- trihydroxy-4*H*-1-benzopyran-4-one) was purchased from SinoPharm Chemical Reagents Co. Ltd., China. Its purity was 0.9965 (mass fraction) as checked by HPLC. Poly(vinylpyrrolidone) (PVP) K30 (CAS. no. 9003-39-8, with IUPAC name 1-ethenylpyrrolidin-2-one and a 0.985 mass fraction purity) was also received from SinoPharm Chemical Reagents Co. Ltd. The main impurity in PVP is water. All samples were dried under vacuum at 333 K for 48 h before use.

Preparation of Samples. Quercetin and PVP K30 were accurately weighed, mixed, and dissolved in the desired amount

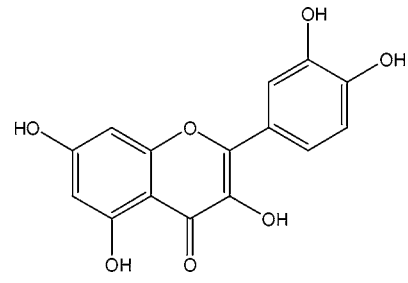

Figure 1. Chemical structure of quercetin. The IUPAC name is 2-(3,4-dihydroxyphenyl)-3,5,7-trihydroxy-4*H*-1-benzopyran-4-one.

* Corresponding author. E-mail: tcbai@suda.edu.cn. Tel: 86-512-65110363. Fax: 86-512-65880089.
[†] Soochow University.
[‡] State University of New York.

10.1021/je1008203
Published on Web 11/30/2010

of ethanol in a closed glass weighing bottle. The mass fractions of quercetin, w_1, of solid samples are 0.1003, 0.1998, 0.2998, 0.3996, 0.5000, 0.5999, 0.7001, 0.7998, and 0.8998. After complete dissolution in ethanol, the solvent was evaporated under reduced pressure at about 313 K in a rotary evaporator. All samples were dried under vacuum at 333 K over 48 h and then were stored over P_2O_5 in a desiccator before use.

DSC Analysis and Heat Capacity Measurements. The heat capacity was measured with a differential scanning calorimeter (NETSCH, DSC-204F1, Germany). Certified indium wire encapsulated in an aluminum crucible was used for temperature and heat flow calibration. An empty aluminum pan and lid were used as the reference for all measurements. Nitrogen gas with a purity of 0.99999 (volum fraction) was used as a purge gas at a rate of 20 mL·min^{-1}, and protective gas was used at 70 mL·min^{-1} in operation. Samples of about 5 mg were weighed to ±0.01 mg using a balance (model BT25S, Sartorius AG, Beijing). A thin disk of sapphire was used as the heat capacity standard.

The measurement of heat capacity included three runs.[18,19,22] An empty Al pan with a lid was the first run used to obtain the baseline. The second and third runs were performed on sapphire and the sample, respectively. One empty Al pan was used throughout three runs. A three-segment heating program was used in DSC operation. The first segment lasting for 15 min was an isothermal one at the initial temperature; the second segment was a dynamic one with a heating rate of 5 K·min^{-1}, and the final segment lasting for 15 min was another isothermal one at the final temperature. The heat capacity is calculated from eq 1.

$$C_{p,\mathrm{sam}} = C_{p,\mathrm{std}}\frac{(\mathrm{DSC_{sam}} - \mathrm{DSC_{bsl}})m_{\mathrm{std}}}{(\mathrm{DSC_{std}} - \mathrm{DSC_{bsl}})m_{\mathrm{sam}}} \quad (1)$$

where $C_{p,\mathrm{sam}}$/J·K^{-1}·g^{-1} and $C_{p,\mathrm{std}}$/J·K^{-1}·g^{-1} are the heat capacity of the sample and the standard substance (sapphire), respectively. $\mathrm{DSC_{sam}}$, $D\mathrm{SC_{bsl}}$, and $\mathrm{DSC_{std}}$ are the heat flows of the sample, baseline, and sapphire runs, respectively, and m_{std} and m_{sam} are the masses of the standard substance and sample, respectively.

Thermogravimetric Analysis. Thermogravimetric (TG) analysis was used to determine the mass loss during the process of temperature programming. The TG experiment was performed with a TA Instruments SDT 2960 in a dynamic flow of nitrogen (0.99999 volume fraction). The gas flow rate was 100 mL·min^{-1}. Approximately (1 to 2) mg of sample was weighed in an aluminum pan and heated from room temperature to 1073 K at a rate of 10 K·min^{-1}, and the loss of weight was recorded.

X-ray Powder Diffraction. An X-ray powder diffraction (XRD) investigation was performed with an X'Pert model PRO MPD diffractometer (PANalytical Company): Cu Kα, λ = 0.15406 nm, voltage 40 kV, and 40 mA, with an angular range of $5 < 2\theta < 60°$ in step scan mode (step width 0.03).

Infrared Spectroscopy. Fourier transform infrared (FT-IR) spectra were obtained on a Magna 550 FT-IR system (Nicolet) with the KBr disk method. The scanning range was (400 to 4000) cm^{-1}, and the resolution was 2 cm^{-1}.

Results and Discussions

Thermal Analysis for Pure PVP K30 and Quercetin. To set up the experimental steps and operating conditions for measuring the heat capacity, the thermal behavior of pure PVP and quercetin was analyzed first.

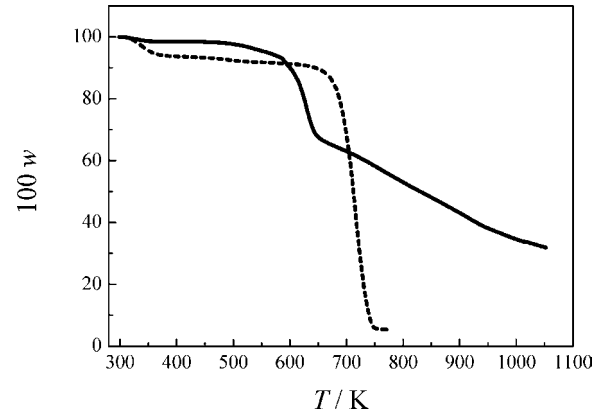

Figure 2. Thermogravimetric trails (mass loss with rising temperature T, w is mass fraction) of quercetin (−) and PVP K30 (---).

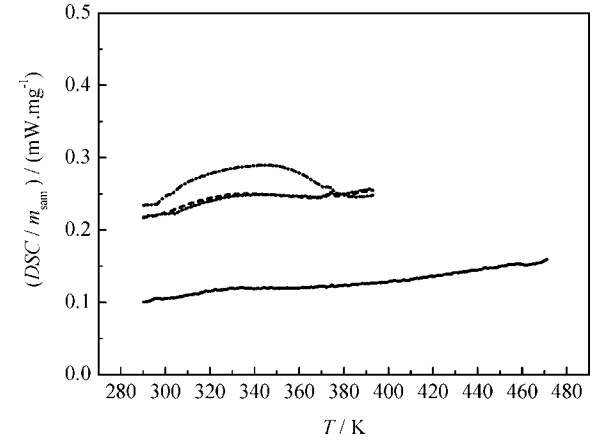

Figure 3. DSC curves of four repeated scans of pure quercetin. The first three (-·-, ---, and − − −) scans ($\mathrm{DSC_{sam}}/m_{\mathrm{sam}}$) were run to evaporate water, and the fourth (−) scan [$(\mathrm{DSC_{sam}} - \mathrm{DSC_{bsl}})/m_{\mathrm{sam}}$] was recorded to evaluate the heat capacity.

The TG trail of quercetin is shown in Figure 2. The mass loss due to water evaporation is found below 393.15 K. As temperature rises to 493.15 K, molecular decomposition is observed. In Figure 2, the TG trail of PVP K30 is shown. Water evaporation is found below 393.15 K, and the temperature of molecule decomposition starts at 633.15 K. This agrees with the report in the literature.[23] If we prepare solid samples carefully, the mass loss due to water evaporation can be reduced to less than 2%. Therefore, in the process of measuring the heat capacity for samples of (quercetin + PVP K30) by DSC, the temperature program should be controlled to below 473.15 K to avoid molecule decomposition, and the effect of water evaporation should be taken into consideration.

In this experiment, all samples were dried under vacuum at 333 K for 48 h before DSC studies. However, during the process of sample weighing and loading into crucibles, the sample will absorb moisture because of the hygroscopicity of PVP K30. Therefore, in the interval after the sample was loaded into the DSC instrument and the C_p measurement had not been made, water was removed under the protection of nitrogen gas. A crucible with a lid containing a pinhole was used in DSC detection. The DSC curves of pure quercetin and PVP K30 are shown in Figures 3 and 4, respectively. Both exhibit a broad endothermic peak due to water evaporation below 393.2 K. Repeated scans lead to peak depression and disappearance. The result of four repeat scans is shown in these Figures. In Figure 3, the first three scans are shown as $\mathrm{DSC_{sam}}/m_{\mathrm{sam}}$ of pure quercetin. The fourth scan is recorded to measure the heat

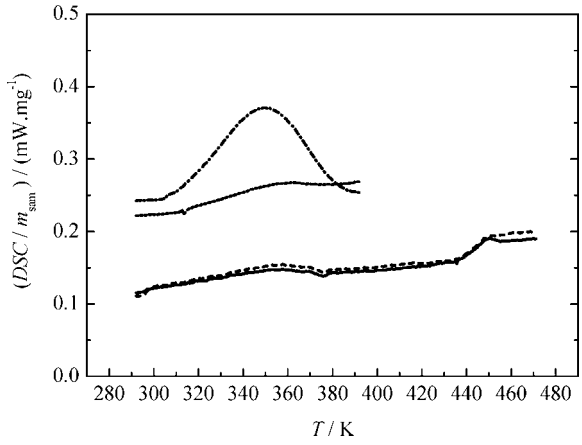

Figure 4. DSC curves of four repeated scans of pure PVP K30. The first (-·-) and second (---) scans (DSC_{sam}/m_{sam}) were run to evaporate water. The third (− − −) and fourth (−) scans [$(DSC_{sam} - DSC_{bsl})/m_{sam}$] were recorded to evaluate the heat capacity.

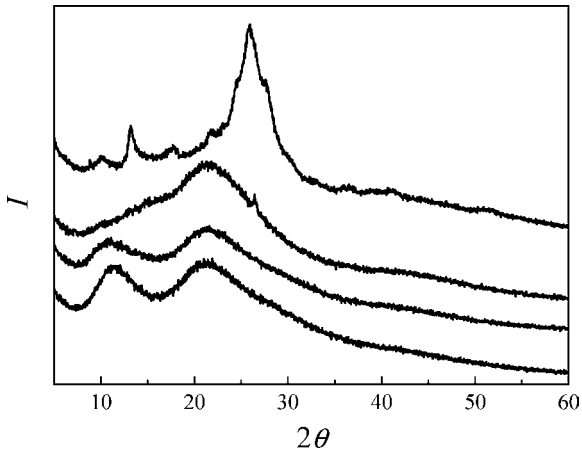

Figure 5. X-ray diffraction patterns (diffraction peak intensity I appearing at angles of 2θ) of [quercetin (1) + PVP K30 (2)] mixtures with mass fractions of $w_1 = 1$, 0.50, 0.10, and 0 (in order from top to bottom).

capacity, $(DSC_{sam} - DSC_{bsl})/m_{sam}$. The trail of the third scan almost overlaps the second scan, which indicates that the effect of water evaporation is minimized and can be neglected. According to this observation, we set up our experimental steps in which the heat capacity is measured after three DSC scans. Figure 4 shows the DSC curves of PVP K30. The first two scans were DSC_{sam}/m_{sam} and were run to remove water, and the third and fourth scans were $(DSC_{sam} - DSC_{bsl})/m_{sam}$ and were recorded to evaluate the heat capacity, which is overlapped as expected.

X-ray Powder Diffraction. XRD gives information about the effect of the degree of crystalline on the solid state. Figure 5 shows the XRD patterns of quercetin, PVP K30, and samples of solid dispersions with $w_1 = 0.1$ and 0.5. Figure 5a is the pattern of pure quercetin in which the distinct sharp peaks indicate that quercetin appears to be a crystalline material with characteristic diffraction peaks appearing at angles of $2\theta =$ (10.38, 13.22, 17.70, 21.98, and 26.12)°. Figure 5d, containing the pattern of PVP K30, shows two broadened peaks that correspond to an amorphous solid state. Figure 5c shows a pattern of quercetin dispersed into PVP with $w_1 = 0.1$. Because there is no sharp peak attributed to crystalline quercetin, Figure 5c suggests that quercetin is in the amorphous state of PVP.[12] Because $w_1 > 0.5$, as shown in Figure 5b, the sharp peak attributed to the pattern of quercetin gradually appears, which indicates that excess quercetin is not embedded into the solid dispersion of PVP. The limit to disperse quercetin into PVP is estimated to be $w_1 < 0.50$.

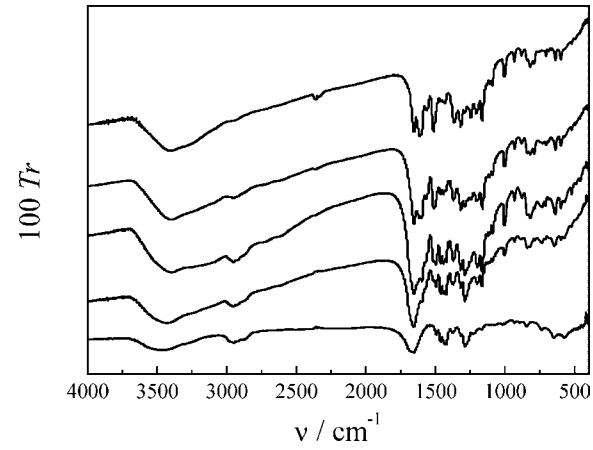

Figure 6. FT-IR spectra (transmittance Tr vs wavenumber ν) of mixtures of [quercetin(1) + PVP K30 (2)] with mass fractions of $w_1 = 1$, 0.70, 0.50, 0.20, and 0 (in order from top to bottom).

FT-IR Spectroscopy. Infrared spectra were recorded in order to tell us if there are possible interactions and reactions between quercetin and PVP in the solid state. The infrared spectra of quercetin, PVP K30, and some of their mixtures are shown in Figure 6.

For quercetin, the band at 3400 cm^{-1} is assigned to a free −OH bond vibration, 2958 cm^{-1} is assigned to the stretching vibration of C−H, 1648 cm^{-1} and 1603 cm^{-1} are assigned to the stretching vibration of the band of the C═O group that appears as a very strong doublet, 1510 cm^{-1} is assigned to an aromatic group, 1312 cm^{-1} and 1164 cm^{-1} are assigned to the C−O−C vibration, and 990 cm^{-1} is assigned to C−H of the aromatic group bending vibration.[24]

The spectrum of PVP K30 shows, among others, important bands at 2950 cm^{-1} (C−H stretch), 1660 cm^{-1} (C═O), and 1280 cm^{-1}(C−N). A broad band is visible at 3450 cm^{-1}, which is attributed to the presence of water.

When a possible interaction is expected between quercetin and PVP K30, it should involve the O−H group of quercetin and the carbonyl group of the polymer involved in hydrogen bonding. Figure 6 shows the spectra of a solid dispersion at $w_1 = 0.20$ in comparison to an uncompletely dispersed solid at $w_1 = 0.70$. Obviously, a band shift was not observed for those bands of quercetin. This indicates that a chemical reaction is not observed between PVP and quercetin. The double bands at 1648 cm^{-1} and 1603 cm^{-1}, which were assigned to the Ar−C═O group of quercetin at $w_1 = 0.70$, were substituted with a large band at 1660 cm^{-1} in the case of $w_1 = 0.20$, which was attributed to the C═O group of PVP. This observation is taken as a consequence of the solid dispersion in which the hydrogen bond between the OH and C═O groups of quercetin was replaced by the interaction between quercetin and PVP. Some bands that decreased in intensity or even disappeared from the spectra of the solid dispersion are consequence of the decrease in w_1. At $w_1 = 0.50$, a tiny excess amount of crystalline quercetin can be evaluated.

Heat Capacity and Solid Dispersion. The specific heat capacities C_p for samples of (quercetin + PVP K30) were measured at temperatures ranging from 298.15 to 473.15 K by DSC. Binary samples with a mass fraction, w_1, from 0.1 to 0.9

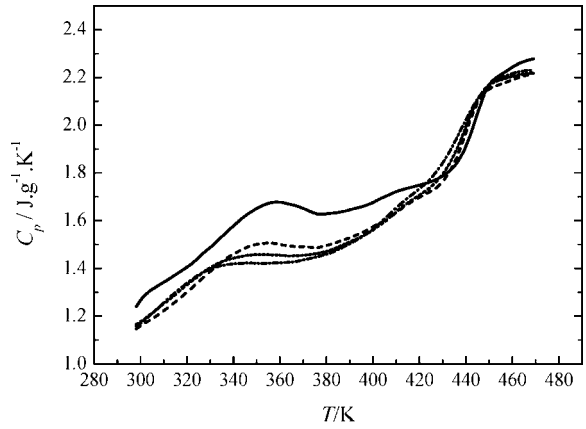

Figure 7. C_p curves against temperature T/K for [quercetin (1) + PVP K30 (2)] with mass fractions of $w_1 = 0$ (−), 0.20 (− − −), 0.40 (---), and 0.50 (-•-) by DSC.

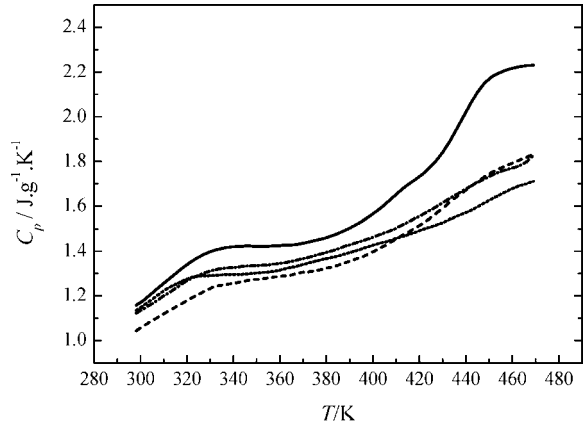

Figure 8. C_p curves against temperature T/K for [quercetin (1) + PVP K30 (2)] with mass fractions of w_1= 1 (-•-), 0.90 (---), 0.70 (− − −) and 0.50 (−) by DSC.

were prepared by the method used to prepare solid dispersions. To eliminate the influence of water, the DSC scan was run repeatedly three times from ambient temperature to 393.2 K, and then C_p was measured during the fourth run. The C_p data are listed in the Supporting Information. The C_p curves can be classified into two types according to their curve features. One is the curves of the solid dispersion with a shape similar to that of pure PVP K30. Another is curves with the shape of the mixed solid dispersion and crystalline quercetin. Figures 7 and 8 show these two types of curves, respectively.

For pure PVP K30, the dependence of C_p on temperature is shown in Figure 7. It can be divided into three segments according to its curve features. In the lower temperature range below 373 K, C_p increases with increasing temperature. In spite of the fact that the sample has been dried carefully and the DSC scan was performed four times, a weak, broad peak at T_{PEAK} = 358.5 K is still observable. This small peak is not attributed to water evaporation or to the solid melting. It may be due to a structure transform that is not clearly known. After this peak, C_p decreased in some extent and then began a new segment. At a temperature above 433.2 K, a glass transition is observed. The temperature of the inflection point T_{INF} is evaluated to be 444.7 K. The third section is in the region of $T > T_{INF}$.

Figure 7 shows the C_p curves of samples with $w_1 \leq 0.5$. In this composition region, samples exist in a state of an amorphous solid dispersion similar to PVP K30. This has been confirmed by the XRD patterns. The curve shapes of these samples are similar to the shape of PVP. The magnitude of the small peak at T_{PEAK} and the inflection point at T_{INF} gradually changes with w_1. The data for T_{PEAK} and T_{INF} for samples with different w_1 values is given in Table 1. Figure 9 shows that, at $w_1 \leq 0.5$, T_{PEAK} decreases slightly with increasing w_1, whereas the change in T_{INF} is not observable.

Table 1. Temperaturesof the Inflection Point (T_{INF}/K) and the Endothermic Peak (T_{PEAK}/K) for [Quercetin (1) + PVP K30 (2)]

w_1	T_{PEAK}/K	T_{INF}/K	w_1	T_{PEAK}/K	T_{INF}/K
0	358.5	444.7	0.50		438.4
0.10	361.2	439.3	0.60		455.4
0.20	355.3	440.3	0.70		464.7
0.30	351.5	440.5	0.80		460.9
0.40	351.3	440.4	0.90		463.7
			1		459.7

Figure 8 gives the C_p curves of quercetin and solid mixtures with w_1 = (0.90, 0.70, and 0.50). The endothermic peak at T_{PEAK} and the glass transition have disappeared. However, another inflection point attributed to quercetin is found in the higher-temperature region, which can be used as a sign to express the mixing behavior between quercetin and the solid dispersion. A gradual transformation from the quercetin crystal to the solid dispersion is observed. The effect of w_1 on the inflection point (T_{INF}) is shown in Figure 9 for $w_1 > 0.5$. The curve of T_{INF} versus w_1 is similar in shape to the phase diagram of the solid−liquid phase equilibrium of binary mixtures with a eutectic composition at $w_1 = 0.50$.

The glass transition is a relaxation phenomenon for the polymer transition from its amorphous solid state to a thawed frozen state. It belongs to the second phase transition. X-ray results indicate that quercetin is no longer present as a crystalline material when its concentration is below $w_1 = 0.50$ but is converted into an amorphous state. The relationship between T_{INF} and w_1 reveals that T_{INF} is nearly unchanged in the region of w_1 = (0.10 to 0.50). However, for mixtures of $w_1 > 0.50$, T_{INF} increases with w_1, where a minimum point similar to the eutectic point is evaluated at $w_1 = 0.50$. Figure 9 suggest that if one wishes to prepare a solid dispersion of (quercetin + PVP K30) to improve the drug efficiency, the composition should be controlled to $w_1 < 0.5$.

Equations to Fit the Heat Capacity. There are many empirical equations to correlate the C_p data with temperature and composition.[18−20,22] For example, the dependence of C_p

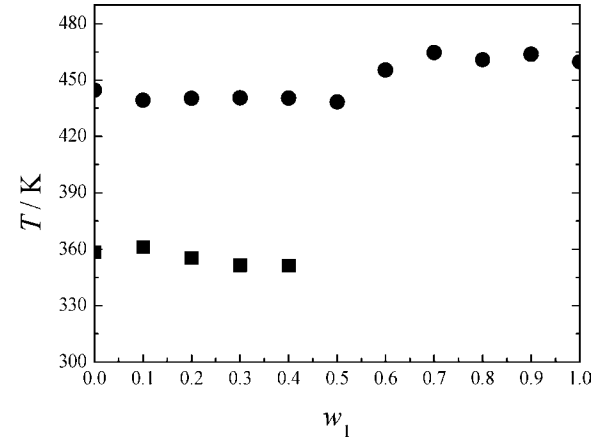

Figure 9. Dependence of T_{INF}/K (•, temperature of the inflection point) and T_{PEAK}/K (■, temperature of the endothermic peak) on the mass fraction of w_1 for [quercetin (1) + PVP K30 (2)].

Table 2. Coefficients of Equation 4 in the Mass Fraction Region of w_1 = (0 to 0.40) and Two Temperature Ranges of (308.2 to 348.2) K and (378.2 to 438.2) K and the Standard Error of the Fit *s*

T_L to T_U (308.2 to 348.2) K							
a_{11}	1.258	a_{21}	0.3410	a_{31}	−0.02661	a_{41}	0.07903
a_{12}	−2.012	a_{22}	−0.3520	a_{32}	1.268	a_{42}	−1.269
a_{13}	9.498	a_{23}	1.389				
a_{14}	−12.51	a_{24}	−3.090				
s	0.008						
T_L to T_U (378.2 to 438.2) K							
a_{11}	1.651	a_{21}	−0.3100	a_3	1.833	a_4	−2.873	a_5	1.599
a_{12}	−2.481	a_{22}	1.948						
a_{13}	11.43	a_{23}	−8.763						
a_{14}	−15.90	a_{24}	13.07						
s	0.017								

Table 3. Coefficients of Equation 4 in the Mass Fraction Region of w_1 = (0.50 to 1) and the Temperature Range of (298.2 to 453.2) K and the Standard Error of the Fit *s*

a_{11}	1.105	a_{21}	1.767	a_{31}	−5.222	a_{41}	7.157	a_{51}	−3.083
a_{12}	0.1284	a_{22}	−2.325	a_{32}	4.681	a_{42}	−6.488	a_{52}	2.506
a_{13}	−2.850	a_{23}	10.54	a_{33}	−12.38	a_{43}	11.41		
a_{14}	5.502	a_{24}	−8.676						
s	0.014								

on temperature can be expressed by eq 2 in the range from a lower temperature T_L to an upper temperature T_U.

$$C_p/\mathrm{J\cdot g^{-1}} = a_1 + a_2x + a_3x^2 + a_4x^3 + a_5x^4 \qquad (2)$$

where

$$x = \frac{T - T_L}{T_U - T_L} \qquad (3)$$

However, for a binary system, a_i will vary with w_1 and the phase state. In this work, three special compositions should be paid more attention; they are w_1 = (0, 0.50, and 1). For pure PVP K30, the C_p curve was divided into three regions because of the curve features, that is, ($T_L \le T < T_{PEAK}$), ($T_{PEAK} < T < T_{INF}$), and ($T > T_{INF}$). To avoid the difficulty encountered in the range of $T > T_{INF}$, the fit of C_p against T by eq 2 is performed within two temperature ranges, $T_L \le T < T_{PEAK}$ and $T_{PEAK} < T < T_{INF}$. For pure quercetin, the C_p curve was divided into two regions at the inflection point. To avoid the difficulty encountered in the range of $T > T_{INF}$, the fit was performed within the range from T_L to T_{INF}. For w_1 = 0.50, the peak in the lower temperature region disappears and its C_p curve has a pattern similar to that of querectin. For solid dispersions with $w_1 < 0.5$, the C_p curves are similar to those of PVP. For solid mixtures of $w_1 \ge 0.50$, C_p curves result from the mixing of quercetin and a solid dispersion of the eutectic composition at w_1 = 0.50. According to this analysis, the process used to correlate coefficient a_i with w_1 is performed within two composition regions: w_1 = (0 to 0.40) and (0.50 to 1).

Equation 4 can be used to relate coefficient a_i to w_1.

$$a_i = a_{i1} + a_{i2}w_1 + a_{i3}{w_1}^2 + a_{i4}{w_1}^3 \qquad (4)$$

Obviously, the coefficient (a_{ij}) is dependent upon the state of solid mixing. By fitting the experimental data using a nonlinear least-squares method in two composition regions and two temperature ranges, a_{ij} coefficients are obtained. In the region of w_1 = (0 to 0.40), a_{ij} values are obtained in two temperature ranges and are provided in Table 2. In the composition region of w_1 = (0.50 to 1), the a_{ij} coefficients are obtained in one temperature range from (298.15 to 453.15) K. The fitting results are listed in Table 3.

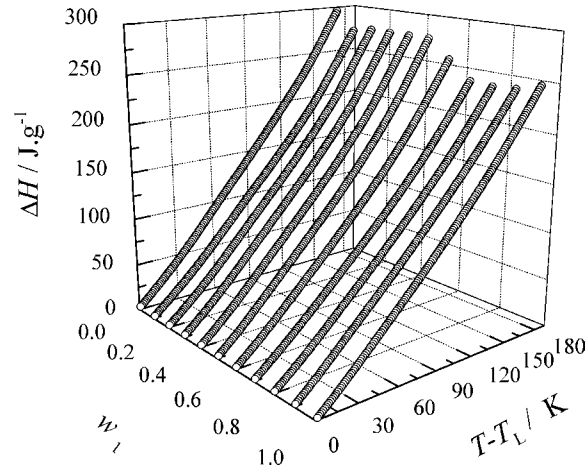

Figure 10. Change in enthalpy ΔH of [quercetin (1) + PVP K30 (2)] from the initial temperature T_L to temperature T as calculated with eq 5.

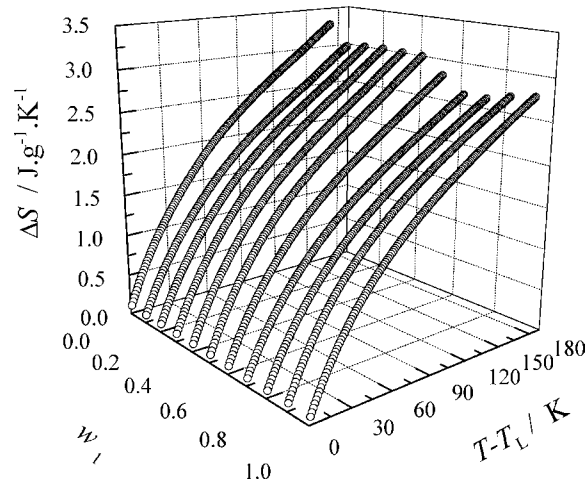

Figure 11. Change of entropy ΔS of [quercetin (1) + PVP K30 (2)] from the initial temperature T_L to temperature T as calculated with eq 6.

Thermodynamic Properties. The change in thermodynamic properties, from the initial temperature T_L to a given temperature T, can be calculated from the C_p data. Thermodynamic relations are given as below.

$$\Delta H = \int_{T_L}^{T} C_p \, \mathrm{d}T \qquad (5)$$

$$\Delta S = \int_{T_L}^{T} \frac{C_p}{T} \, \mathrm{d}T \qquad (6)$$

H and S are the enthalpy and entropy, respectively. The results of the calculation are graphically shown in Figures 10 and 11.

Conclusions

The heat capacity of a solid mixture is an essential piece of data in predicting the thermodynamic properties and the phase state. It is valuable in the evaluation of the efficiency of solid dispersions of drugs. For the system [quercetin (1) + PVP K30 (2)], a solid dispersion is formed in the $w_1 < 0.50$ region, where w_1 is the mass fraction of quercetin. In this region, a glass

transition in the higher-temperature region and a small endothermic peak in the lower-temperature region attributed to PVP are observed, and quercetin is present in the amorphous state of PVP. However, in the $w_1 > 0.5$ region, another inflection point not attributed to the glass transformation is found, and a mixture of crystalline quercetin with an amorphous solid dispersion is observed.

The dependence of C_p on T is expressed by a polynomial equation. The polynomial coefficients are dependent upon w_1 and the solid mixing state. The changes in enthalpy and entropy with temperature were calculated from C_p.

Supporting Information Available:

Experimental C_p data. This material is available free of charge via the Internet at http://pubs.acs.org.

Literature Cited

(1) Firuzi, O.; Lacanna, A.; Petrucci, R.; Marrosu, G.; Saso, L. Evaluation of the antioxidant activity of flavonoids by "ferric reducing antioxidant power" assay and cyclic voltammetry. *Biochim. Biophys. Acta* **2005**, *1721*, 174–184.

(2) Peng, Z. F.; Strack, D.; Baumert, A.; Subramaniam, R.; Goh, N. K.; Chia, T. F.; Tan, S. N.; Chia, L. S. Antioxidant flavonoids from leaves of *Polygonum hydropiper* L. *Phytochemistry* **2003**, *62*, 219–228.

(3) Chen, Z. Y.; Chan, P. T.; Ho, K. Y.; Fung, K. P.; Wang, J. Antioxidant activity of natural flavonoids is governed by number and location of their aromatic hydroxyl groups. *Chem. Phys. Lipids* **1996**, *79*, 157–163.

(4) Dias, K.; Nikolaou, S.; De Giovani, W. F. Synthesis and spectral investigation of Al(III) catechin/β-cyclodextrin and Al(III) quercetin/β-cyclodextrin inclusion compounds. *Spectrochim. Acta, Part A* **2008**, *70*, 154–161.

(5) Bukhari, S. B.; Memona, S.; Tahir, M. M.; Bhanger, M. I. Synthesis, characterization and investigation of antioxidant activity of cobalt-quercetin complex. *J. Mol. Struct.* **2008**, *892*, 39–46.

(6) Jones, D. J. L.; Jukes-Jones, R.; Verschoyle, R. D.; Farmera, P. B.; Gescher, A. A synthetic approach to the generation of quercetin sulfates and the detection of quercetin 3′-*O*-sulfate as a urinary metabolite in the rat. *Bioorg. Med. Chem.* **2005**, *13*, 6727–6731.

(7) Needs, P. W.; Kroon, P. A. Convenient syntheses of metabolically important quercetin glucuronides and sulfates. *Tetrahedron* **2006**, *62*, 6862–6868.

(8) Bergonzi, M. C.; Bilia, A. R.; Bari, L. D.; Mazzia, G.; Vincieri, F. F. Studies on the interactions between some flavonols and cyclodextrins. *Bioorg. Med. Chem. Lett.* **2007**, *17*, 5744–5748.

(9) Pralhad, T.; Rajendrakumar, K. Study of freeze-dried quercetin-cyclodextrin binary systems by DSC, FT-IR, X-ray diffraction and SEM analysis. *J. Pharm. Biomed. Anal.* **2004**, *34*, 333–339.

(10) Jullian, C.; Moyano, L.; Yañez, C.; Olea-Azar, C. Complexation of quercetin with three kinds of cyclodextrins: an antioxidant study. *Spectrochim. Acta, Part A* **2007**, *67*, 230–234.

(11) Yan, C.; Li, X. H.; Xiu, Z. L.; Hao, C. A quantum-mechanical study on the complexation of β-cyclodextrin with quercetin. *J. Mol. Struct.: THEOCHEM* **2006**, *764*, 95–100.

(12) Zhu, J.; Yang, Z.-G.; Chen, X.-M.; Sun, J.-B.; Awuti, G.; Zhang, X.; Zhang, Q. Preparation and physicochemical characterization of solid dispersion of quercetin and polyvinylpyrrolidone. *J. Chin. Pharm. Sci* **2007**, *16*, 51–56.

(13) Vasconcelos, T.; Sarmento, B.; Costa, P. Solid dispersions as strategy to improve oral bioavailability of poor water soluble drugs. *Drug Discovery Today* **2007**, *12*, 1068–1075.

(14) Blagden, N.; de Matas, M.; Gavan, P. T.; York, P. Crystal engineering of active pharmaceutical ingredients to improve solubility and dissolution rates. *Adv. Drug Delivery Rev.* **2007**, *59*, 617–630.

(15) Alsenz, J.; Kansy, M. High throughput solubility measurement in drug discovery and development. *Adv. Drug Delivery Rev.* **2007**, *59*, 546–567.

(16) Van den Mooter, G.; Augustijns, P.; Blaton, N.; Kinget, R. Physicochemical characterization of solid dispersions of temazepam with polyethylene glycol 6000 and PVP K30. *Int. J. Pharm.* **1998**, *164*, 67–80.

(17) Liu, Z. H. *Introduction to Thermal Analysis*; Chemical Industry Press: Beijing, 1991.

(18) Hua, X.; Kaplan, D.; Cebe, P. Effect of water on the thermal properties of silk fibroin. *Thermochim. Acta* **2007**, *461*, 137–144.

(19) Xu, K. Z.; Song, J. R.; Zhao, F. Q.; Ma, H. X.; Gao, H. X.; Chang, C. R.; Ren, Y. H.; Hu, R. Z. Thermal behavior, specific heat capacity and adiabatic time-to-explosion of G(FOX-7). *J. Hazard. Mater.* **2008**, *158*, 333–339.

(20) Tong, B.; Tan, Z.-C.; Shi, Q.; Li, Y.-S.; Yue, D.-T.; Wang, S.-X. Thermodynamic investigation of several natural polyols (I): heat capacities and thermodynamic properties of xylitol. *Thermochim. Acta* **2007**, *457*, 20–26.

(21) Sethia, S.; Squillante, E. Solid dispersion of carbamazepine in PVP K30 by conventional solvent evaporation and supercritical methods. *Int. J. Pharm.* **2004**, *272*, 1–10.

(22) Mundhwa, M.; Elmahmudi, S.; Maham, Y.; Henni, A. Molar heat capacity of aqueous sulfolane, 4-formylmorpholine, 1-methyl-2-pyrrolidinone, and triethylene glycol dimethyl ether solutions from (303.15 to 353.15) K. *J. Chem. Eng. Data* **2009**, *54*, 2895–2901.

(23) Fini, A.; Cavallari, C.; Ospitali, F. Raman and thermal analysis of indomethacin /PVP solid dispersion enteric microparticles. *Eur. J. Pharm. Biopharm.* **2008**, *70*, 409–420.

(24) Xie, J.-X.; Chang, J.-B.; Wang, X.-M. *Infrared Spectroscopy Application in Organic Chemistry and Drug Chemistry*; Science Press.: Beijing, 2001; pp 403−456.

Received for review August 9, 2010. Accepted November 14, 2010.

JE1008203